SANDIA REPORT

SAND98–8403 • UC–1409
Unlimited Release
Printed November 1997

M98050978

On Pulsating and Cellular Forms of Hydrodynamic Instability in Liquid-Propellant Combustion

Stephen B. Margolis

Prepared by
Sandia National Laboratories
Albuquerque, New Mexico 87185 and Livermore, California 94550

Sandia is a multiprogram laboratory operated by Sandia Corporation, a Lockheed Martin Company, for the United States Department of Energy under Contract DE-AC04-94AL85000.

Sandia National Laboratories

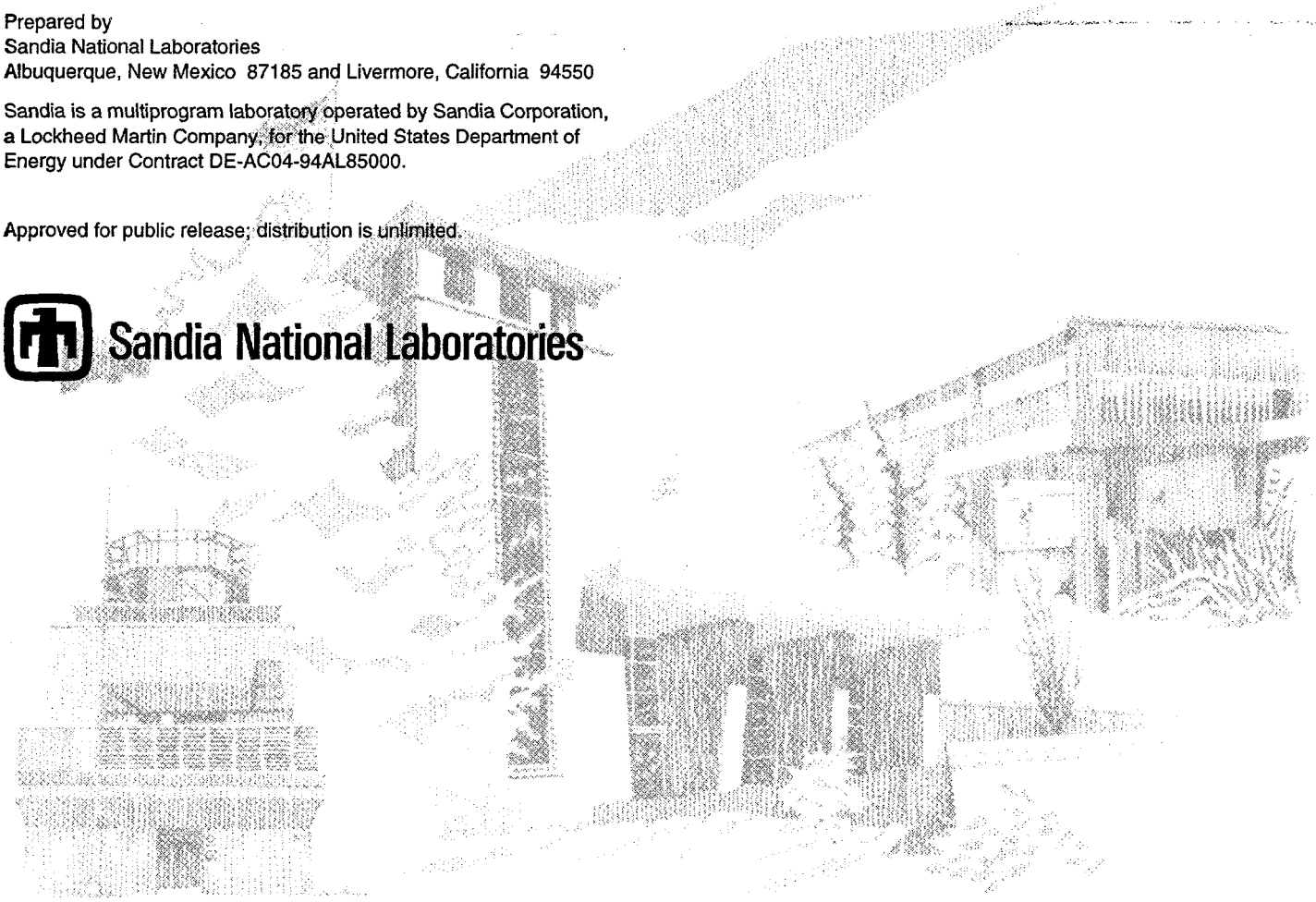

Issued by Sandia National Laboratories, operated for the United States Department of Energy by Sandia Corporation.

Available to DOE and DOE contractors from
Office of Scientific and Technical Information
P.O. Box 62
Oak Ridge, TN 37831

Prices available from (615) 576-8401, FTS 626-8401

Available to the public from
National Technical Information Service
U.S. Department of Commerce
5285 Port Royal Rd
Springfield, VA 22161

NTIS price codes
Printed copy: A03
Microfiche copy: A01

SAND98-8403 • UC-1409
Unlimited Release
Printed November 1997

ON PULSATING AND CELLULAR FORMS OF HYDRODYNAMIC INSTABILITY IN LIQUID-PROPELLANT COMBUSTION

STEPHEN B. MARGOLIS
Combustion Research Facility, MS 9052
Sandia National Laboratories, Livermore, California 94551-0969

Abstract

An extended Landau/Levich model of liquid-propellant combustion, one that allows for a local dependence of the burning rate on the (gas) pressure at the liquid/gas interface, exhibits not only the classical hydrodynamic cellular instability attributed to Landau, but also a pulsating hydrodynamic instability associated with sufficiently negative pressure sensitivities. Exploiting the realistic limit of small values of the gas-to-liquid density ratio ρ, analytical formulas for both neutral stability boundaries may be obtained by expanding all quantities in appropriate powers of ρ in each of three distinguished wavenumber regimes. In particular, composite analytical expressions are derived for the neutral stability boundaries $A_p(k)$, where A_p is the pressure sensitivity of the burning rate and k is the wavenumber of the disturbance. For the cellular boundary, the results demonstrate explicitly the stabilizing effect of gravity on long-wave disturbances, the stabilizing effect of viscosity (both liquid and gas) and surface tension on short-wave perturbations, and the instability associated with intermediate wavenumbers for negative values of A_p, which is characteristic of many hydroxylammonium nitrate-based liquid propellants over certain pressure ranges. In contrast, the pulsating hydrodynamic stability boundary is insensitive to gravitational and surface-tension effects, but is more sensitive to the effects of liquid viscosity since, for typical nonzero values of the latter, the pulsating boundary decreases to larger negative values of A_p as k increases through O(1) values. Thus, liquid-propellant combustion is predicted to be stable (that is, steady and planar) only for a range of negative pressure sensitivities that lie below the cellular boundary that exists for sufficiently small negative values of A_p, and above the pulsating boundary that exists for larger negative values of this parameter.

ON PULSATING AND CELLULAR FORMS OF HYDRODYNAMIC INSTABILITY IN LIQUID-PROPELLANT COMBUSTION

Introduction

The stability of liquid-propellant deflagration is a fundamental problem that was first treated by Landau in a classical study [1] that introduced the concept of hydrodynamic instability in a combustion context. Referred to as the "slow combustion of liquids", that analysis is most applicable to certain realistic limiting cases in which combustion may be approximated by an overall reaction at the liquid/gas interface. For example, the gas flame may occur under near-breakaway conditions, exerting little thermal or hydrodynamic influence on the burning propellant, or distributed combustion may only occur in an intrusive regime such that the reaction zone lies closer to the liquid/gas interface than the length scale of any disturbance of interest, or the liquid propellant may simply undergo exothermic decomposition at the surface without any significant distributed combustion, such as appears to occur in some types of hydroxylammonium nitrate (HAN)-based liquid propellants at low pressures [2]. The results of Landau's study, along with a subsequent paper by Levich [3] that replaced the effects due to surface tension in the earlier study with those due to (liquid) viscosity, have been widely quoted and offer much in terms of physical insight into the nature of this type of instability, which, as in the case of gaseous combustion, is associated with the density change across the reaction front. However, since these models assumed a constant normal burning rate, it has proven useful to improve upon these models by incorporating a more realistic coupling of the normal propagation speed with the local pressure and/or temperature fields, thereby allowing for a locally varying burning rate [4,5]. One result that has emerged from this generalization is that, in addition to the classical Landau (cellular) type of instability, the models now predict a pulsating hydrodynamic instability as well. The latter arises specifically from the local pressure coupling and thus may be physically achievable since the mass burning rate of many propellants has been shown empirically to correlate well with pressure. Thermal coupling, on the other hand, introduces additional thermal/diffusive instabilities [5] that will not be considered here. In the present work, we shall consider both types of hydrodynamic instabilities, but particular focus will be placed on the pulsating stability boundary, since this type of instability is absent from the earlier models that neglected the pressure coupling indicated above. As in a companion study that focused on the the classical (cellular) hydrodynamic instability [6], we develop a formal asymptotic theory by considering the realistic limiting case in which the gas-to-liquid density ratio ρ is small.

Mathematical Model

The governing hydrodynamic equations consist of mass and momentum on either side of the gas/liquid interface, supplemented by a pressure-dependent burning-rate law and associated continuity and jump conditions across the interface [4–6]. Thus, it is assumed, as in the classical models, that there is no distributed reaction in either the liquid or gas phases, but that there exists either a pyrolysis reaction or an exothermic decomposition at the liquid/gas interface that depends on the local pressure. For simplicity, it is assumed that within the liquid and gas phases separately, the density and other fluid properties are constants, with appropriate jumps across the phase boundary. The nondimensional location of the latter is denoted by $x_3 = \Phi_s(x_1, x_2, t)$, where the adopted coordinate system is fixed with respect to the stationary liquid at $x_3 = -\infty$ (Fig. 1). Then, in the moving coordinate system $x = x_1$, $y = x_2$, $z = x_3 - \Phi_s(x_1, x_2, t)$, in terms of which the liquid/gas interface always lies at $z = 0$, the complete nondimensional formulation of the problem in the absence of thermal coupling is given by

$$\nabla \cdot \mathbf{v} = 0\,, \quad z \neq 0\,, \tag{1}$$

$$\frac{\partial \mathbf{v}}{\partial t} - \frac{\partial \Phi_s}{\partial t}\frac{\partial \mathbf{v}}{\partial z} + (\mathbf{v}\cdot\nabla)\mathbf{v} = (0,0,-Fr^{-1}) - \left\{ \begin{matrix} 1 \\ \rho^{-1} \end{matrix} \right\} \nabla p + \left\{ \begin{matrix} Pr_l \\ \lambda Pr_g \end{matrix} \right\} \nabla^2 \mathbf{v}\,, \quad z \lesseqgtr 0\,, \tag{2}$$

subject to $\mathbf{v} = 0$ at $z = -\infty$ and the interface conditions

$$\hat{\mathbf{n}}_\mathbf{s} \times \mathbf{v}_- = \hat{\mathbf{n}}_\mathbf{s} \times \mathbf{v}_+\,, \tag{3}$$

$$\hat{\mathbf{n}}_\mathbf{s} \cdot (\mathbf{v}_- - \rho \mathbf{v}_+) = (1-\rho) S(\Phi_s) \frac{\partial \Phi_s}{\partial t}\,, \tag{4}$$

$$\hat{\mathbf{n}}_\mathbf{s} \cdot \mathbf{v}_- - S(\Phi_s)\frac{\partial \Phi_s}{\partial t} = A(p_+)\,, \tag{5}$$

$$\begin{aligned} p_- - p_+ = {} & \hat{\mathbf{n}}_\mathbf{s} \cdot [\rho \mathbf{v}_+ (\hat{\mathbf{n}}_\mathbf{s} \cdot \mathbf{v}_+) - \mathbf{v}_- (\hat{\mathbf{n}}_\mathbf{s} \cdot \mathbf{v}_-) - \rho \lambda Pr_g \mathbf{e}_+ \cdot \hat{\mathbf{n}}_\mathbf{s} + Pr_l \mathbf{e}_- \cdot \hat{\mathbf{n}}_\mathbf{s}] + \hat{\mathbf{n}}_\mathbf{s} \cdot (\mathbf{v}_- - \rho \mathbf{v}_+) S(\Phi_s) \frac{\partial \Phi_s}{\partial t} \\ & - \gamma S^3(\Phi_s) \left\{ \frac{\partial^2 \Phi_s}{\partial x^2} \left[1 + \left(\frac{\partial \Phi_s}{\partial y} \right)^2 \right] + \frac{\partial^2 \Phi_s}{\partial y^2} \left[1 + \left(\frac{\partial \Phi_s}{\partial x} \right)^2 \right] - 2 \frac{\partial \Phi_s}{\partial x} \frac{\partial \Phi_s}{\partial y} \frac{\partial^2 \Phi_s}{\partial x \partial y} \right\}, \end{aligned} \tag{6}$$

$$\hat{\mathbf{n}}_\mathbf{s} \times \left[\rho \mathbf{v}_+ (\hat{\mathbf{n}}_\mathbf{s} \cdot \mathbf{v}_+) - \mathbf{v}_- (\hat{\mathbf{n}}_\mathbf{s} \cdot \mathbf{v}_-) + (\mathbf{v}_- - \rho \mathbf{v}_+) S(\Phi_s) \frac{\partial \Phi_s}{\partial t} \right] = \hat{\mathbf{n}}_\mathbf{s} \times (\rho \lambda Pr_g \mathbf{e}_+ \cdot \hat{\mathbf{n}}_\mathbf{s} - Pr_l \mathbf{e}_- \cdot \hat{\mathbf{n}}_\mathbf{s})\,, \tag{7}$$

where the latter represent continuity of transverse velocity components (no-slip), conservation of (normal) mass flux, the mass burning-rate law, and conservation of normal and transverse components of momentum flux, respectively. Here, $\mathbf{v}$ and p denote velocity [with respect to the original (x_1, x_2, x_3) coordinate system] and pressure, and the $\pm$ subscripts denote evaluation at $z = 0^\pm$. The parameters Pr_l and Pr_g denote the liquid and gas-phase Prandtl numbers, ρ and λ are the gas-to-liquid density and thermal diffusivity ratios, Fr is the Froude number, $\mathbf{e}$ is the

rate-of-strain tensor and γ is the surface-tension coefficient. All of these quantities are defined in terms of their dimensional counterparts in the nomenclature. In addition, the factor $S(\Phi_s)$ and the unit normal $\mathbf{n}_s$ are given by

$$S(\Phi_s) \equiv \left[1 + (\partial\Phi_s/\partial x)^2 + (\partial\Phi_s/\partial y)^2\right]^{-1/2}, \quad \hat{\mathbf{n}}_\mathbf{s} = (-\partial\Phi_s/\partial x, -\partial\Phi_s/\partial y, 1)S(\Phi_s)\,, \tag{8}$$

while the expressions for the gradient operator ∇ and the Laplacian ∇^2 in the moving coordinate system are given by

$$\nabla = \Big(\frac{\partial}{\partial x} - \frac{\partial\Phi_s}{\partial x}\frac{\partial}{\partial z}, \frac{\partial}{\partial y} - \frac{\partial\Phi_s}{\partial y}\frac{\partial}{\partial z}, \frac{\partial}{\partial z}\Big)\,, \tag{9}$$

$$\nabla^2 = \frac{\partial^2}{\partial x^2} + \frac{\partial^2}{\partial y^2} + \left[1 + \Big(\frac{\partial\Phi_s}{\partial x}\Big)^2 + \Big(\frac{\partial\Phi_s}{\partial y}\Big)^2\right]\frac{\partial^2}{\partial z^2} - 2\frac{\partial\Phi_s}{\partial x}\frac{\partial^2}{\partial x\partial z} - 2\frac{\partial\Phi_s}{\partial y}\frac{\partial^2}{\partial y\partial z} - \Big(\frac{\partial^2\Phi_s}{\partial x^2} + \frac{\partial^2\Phi_s}{\partial y^2}\Big)\frac{\partial}{\partial z}. \tag{10}$$

We remark that the factor multiplying γ in Eq.(6) is the curvature $-\nabla\cdot\hat{\mathbf{n}}$ and note that $\rho\lambda Pr_g = \mu Pr_l$, where is the gas-to-liquid viscosity ratio. In addition, we observe that the burning rate $A(p)$ in Eq. (5) is assumed to depend on the local gas pressure at the interface, where A is normalized to unity for the case of steady, planar burning. Indeed, in what follows, the pressure sensitivity $A_p = \partial A/\partial p$ of the local burning rate will emerge as an important parameter.

A nontrivial basic solution to the above problem, corresponding to the special case of a steady, planar deflagration, is given by

$$\Phi_s^0 = -t\,, \quad \mathbf{v^0} = (0,0,v^0)\,, \quad v^0 = \begin{cases} 0, & z<0 \\ \rho^{-1}-1, & z>0\,, \end{cases} \quad p^0(z) = \begin{cases} -Fr^{-1}z + \rho^{-1} - 1, & z<0 \\ -\rho Fr^{-1}z, & z>0\,. \end{cases} \tag{11}$$

The linear stability analysis of this solution now proceeds in a standard fashion. However, owing to the significant number of parameters, a complete analysis of the resulting dispersion relation is quite complex, and we follow our previous approach [6] by restricting further consideration to the realistic parameter regime $\rho \ll 1$, $\mu \ll 1$, and in the case of microgravity, $Fr^{-1} \ll 1$. In contrast, the earlier classical studies only considered special limiting cases and/or assumptions. Thus, in the study due to Landau [1], viscosity was neglected and the effects of gravity (assumed to act normal to the undisturbed planar interface in the direction of the unburned liquid) and surface tension were shown to be stabilizing, leading to a criterion for the absolute stability for steady, planar deflagration of the form (in our nondimensional notation) $4\gamma Fr^{-1}\rho^2/(1-\rho) > 1$. In the study due to Levich [3], surface tension was neglected, but the effects due to the viscosity of the liquid were included, leading to the absolute stability criterion $Fr^{-1}Pr_l(3\rho)^{3/2} > 1$. Thus, these two studies, both of which assumed a constant normal burning rate ($A = 1$), demonstrated that sufficiently large values of either viscosity or surface tension, when coupled with the effects due to gravity, may render steady, planar deflagration stable to hydrodynamic disturbances. In our recent study [6], these results were synthesized and extended to the more realistic case of a

nonconstant burning rate (*i.e.*, $A_p \neq 0$) in the limiting parameter regime identified above. In the present work, we summarize these results for the classical cellular boundary and use the resulting scalings to derive an expression for the pulsating hydrodynamic stability boundary that arises from the pressure-dependence of the local burning rate.

Linear Stability Problem

With respect to the basic solution (11), the perturbation quantities $\phi_s(x,y,t)$, $\mathbf{u}(x,y,z,t)$ and $\zeta(x,y,z,t)$ are defined as

$$\Phi_s = \Phi_s^0(t) + \phi_s\,, \quad \mathbf{v} = \mathbf{v^0}(z) + \mathbf{u}\,, \quad p = p^0(z) + \zeta\,. \tag{12}$$

Substituting Eqs. (20) into the nonlinear model defined above and linearizing about the basic solution (11), the perturbation problem becomes

$$\frac{\partial u_1}{\partial x} + \frac{\partial u_2}{\partial y} + \frac{\partial u_3}{\partial z} = 0\,, \quad z \neq 0\,, \tag{13}$$

$$\begin{aligned}\left\{\begin{matrix}1\\ \rho\end{matrix}\right\}\frac{\partial \mathbf{u}}{\partial t} + \frac{\partial \mathbf{u}}{\partial z} = &-\left(\frac{\partial \zeta}{\partial x} + \left\{\begin{matrix}1\\ \rho\end{matrix}\right\}Fr^{-1}\frac{\partial \phi_s}{\partial x}, \frac{\partial \zeta}{\partial y} + \left\{\begin{matrix}1\\ \rho\end{matrix}\right\}Fr^{-1}\frac{\partial \phi_s}{\partial y}, \frac{\partial \zeta}{\partial z}\right)\\ &+\left\{\begin{matrix}Pr_l\\ \rho\lambda Pr_g\end{matrix}\right\}\left(\frac{\partial^2 \mathbf{u}}{\partial x^2} + \frac{\partial^2 \mathbf{u}}{\partial y^2} + \frac{\partial^2 \mathbf{u}}{\partial z^2}\right), \quad z \lesseqgtr 0\,,\end{aligned} \tag{14}$$

subject to $\mathbf{u} = \mathbf{0}$ at $z = -\infty$ and

$$u_1\big|_{z=0^-} - u_1\big|_{z=0^+} = (\rho^{-1} - 1)\frac{\partial \phi_s}{\partial x}\,, \tag{15}$$

$$u_2\big|_{z=0^-} - u_2\big|_{z=0^+} = (\rho^{-1} - 1)\frac{\partial \phi_s}{\partial y}\,, \tag{16}$$

$$u_3\big|_{z=0^-} - \rho u_3\big|_{z=0^+} = (1 - \rho)\frac{\partial \phi_s}{\partial t}\,, \tag{17}$$

$$u_3\big|_{z=0^-} - \frac{\partial \phi_s}{\partial t} = A_p \zeta|_{z=0^+}\,, \tag{18}$$

$$\zeta|_{z=0^-} - \zeta|_{z=0^+} = 2\left(u_3\big|_{z=0^+} - u_3\big|_{z=0^-}\right) + 2Pr_l\left(\frac{\partial u_3}{\partial z}\bigg|_{z=0^-} - \mu\frac{\partial u_3}{\partial z}\bigg|_{z=0^+}\right) - \gamma\left(\frac{\partial^2 \phi_s}{\partial x^2} + \frac{\partial^2 \phi_s}{\partial y^2}\right), \tag{19}$$

$$\mu Pr_l\left(\frac{\partial u_1}{\partial z}\bigg|_{z=0^+} + \frac{\partial u_3}{\partial x}\bigg|_{z=0^+}\right) - Pr_l\left(\frac{\partial u_1}{\partial z}\bigg|_{z=0^-} + \frac{\partial u_3}{\partial x}\bigg|_{z=0^-}\right) = 0\,, \tag{20}$$

$$\mu Pr_l\left(\frac{\partial u_2}{\partial z}\bigg|_{z=0^+} + \frac{\partial u_3}{\partial y}\bigg|_{z=0^+}\right) - Pr_l\left(\frac{\partial u_2}{\partial z}\bigg|_{z=0^-} + \frac{\partial u_3}{\partial y}\bigg|_{z=0^-}\right) = 0\,, \tag{21}$$

where Eqs. (15) – (17) have been used to simplify Eqs. (19) – (21).

Nontrivial harmonic solutions for ϕ_s, $\mathbf{u}$ and ζ, proportional to $e^{i\omega t+ik_1x+ik_2y}$, that satisfy Eqs. (21) - (22) and the boundary/boundedness conditions at $z=\pm\infty$ are given by

$$\phi_s = e^{i\omega t+ik_1x+ik_2y}\,, \tag{22}$$

$$\zeta = e^{i\omega t+ik_1x+ik_2y}\begin{cases} b_1e^{kz}-Fr^{-1}, & z<0 \\ b_2e^{-kz}-\rho Fr^{-1}, & z>0\,, \end{cases} \tag{23}$$

$$u_1 = e^{i\omega t+ik_1x+ik_2y}\begin{cases} b_3e^{qz}-ik_1(i\omega+k)^{-1}b_1e^{kz}, & z<0 \\ b_4e^{rz}-ik_1(i\omega\rho-k)^{-1}b_2e^{-kz}, & z>0\,, \end{cases} \tag{24}$$

$$u_2 = e^{i\omega t+ik_1x+ik_2y}\begin{cases} b_5e^{qz}-ik_2(i\omega+k)^{-1}b_1e^{kz}, & z<0 \\ b_6e^{rz}-ik_2(i\omega\rho-k)^{-1}b_2e^{-kz}, & z>0\,, \end{cases} \tag{25}$$

$$u_3 = e^{i\omega t+ik_1x+ik_2y}\begin{cases} b_7e^{qz}-k(i\omega+k)^{-1}b_1e^{kz}, & z<0 \\ b_8e^{rz}+k(i\omega\rho-k)^{-1}b_2e^{-kz}, & z>0\,, \end{cases} \tag{26}$$

where the above solution has been normalized by setting the coefficient of the harmonic dependence of ϕ_s to unity. Here, the signs of k_1 and k_2 may be either positive or negative, and we have employed the definitions $k=\sqrt{k_1^2+k_2^2}$, and q and r are defined as

$$2Pr_l\,q = 1+\sqrt{1+4Pr_l(i\omega+Pr_l\,k^2)}\,, \tag{27}$$

$$2\mu Pr_l\,r = 1-\sqrt{1+4\mu Pr_l(i\omega\rho+\mu Pr_l\,k^2)}\,. \tag{28}$$

Substituting this solution into the interface conditions (15) - (21) and using Eq. (13) for $z\lesseqgtr 0$ yields nine conditions for the eight coefficients b_1 - b_8 and the complex frequency (dispersion relation) $i\omega(k)$. In particular, these conditions are given by

$$ik_1b_3+ik_2b_5+qb_7=0\,, \tag{29}$$

$$ik_1b_4+ik_2b_6+rb_8=0\,, \tag{30}$$

$$b_3-\frac{ik_1}{i\omega+k}b_1-b_4+\frac{ik_1}{i\omega\rho-k}b_2=\Big(\frac{1}{\rho}-1\Big)ik_1\,, \tag{31}$$

$$b_5-\frac{ik_2}{i\omega+k}b_1-b_6+\frac{ik_2}{i\omega\rho-k}b_2=\Big(\frac{1}{\rho}-1\Big)ik_2\,, \tag{32}$$

$$b_7-\frac{k}{i\omega+k}b_1-\rho b_8-\frac{\rho k}{i\omega\rho-k}b_2=(1-\rho)i\omega\,, \tag{33}$$

$$b_7-\frac{k}{i\omega+k}b_1-A_p\,b_2=i\omega-\rho Fr^{-1}A_p\,, \tag{34}$$

$$\begin{aligned}\Big[1+\frac{k}{i\omega+k}(2kPr_l-1)\Big]b_1-\Big[1+\frac{k}{i\omega\rho-k}(2k\mu Pr_l+2-\rho)\Big]b_2 \\ +(1-2Pr_l\,q)b_7-(2-\rho-2\mu Pr_l\,r)b_8=(1-\rho)(Fr^{-1}-i\omega)+\gamma k^2\,,\end{aligned} \tag{35}$$

$$(\mu Pr_l\, r-1)b_4+(2k\mu Pr_l+1)\frac{ik_1}{i\omega\rho-k}b_2+ik_1\mu Pr_l\, b_8$$
$$+(1-Pr_l\, q)b_3+(2Pr_l\, k-1)\frac{ik_1}{i\omega+k}b_1-ik_1Pr_l\, b_7=\Big(\frac{1}{\rho}-1\Big)ik_1\,, \tag{36}$$

$$(\mu Pr_l\, r-1)b_6+(2k\mu Pr_l+1)\frac{ik_2}{i\omega\rho-k}b_2+ik_2\mu Pr_l\, b_8$$
$$+(1-Pr_l\, q)b_5+(2Pr_l\, k-1)\frac{ik_2}{i\omega+k}b_1-ik_2Pr_l\, b_7=\Big(\frac{1}{\rho}-1\Big)ik_2\,. \tag{37}$$

Although the above problem is linear in the coefficients b_1 - b_8, explicit expressions for the dispersion relation $i\omega(k)$ and the neutral stability boundaries, are not readily obtainable in closed form, except in certain special cases as noted below. However, it is possible to develop tractable perturbation expansions for these quantities in the realistic limit that the density and viscosity ratios ρ and μ are small, as is Fr^{-1} in the case of reduced gravity.

Asymptotic Analysis of the Cellular Stability Boundary

It turns out that the $\rho \ll 1$ limit implies the existence of several different wavenumber regimes [6], which in turn implies several different expansions for the dispersion relation. This is motivated by considering the solution of (29) – (37) in the limit of zero viscosity ($\mu - Pr_l = 0$), which leads to a tractable form of the dispersion relation for arbitrary ρ. In particular, the neutral stability boundaries with respect to infinitesimal hydrodynamic disturbances proportional to $e^{i\omega t \pm i\mathbf{k}\cdot\mathbf{x}}$, where $\mathbf{k}$ and $\mathbf{x}$ are the transverse wavenumber and coordinate vectors, respectively, are given for $A_p < 0$ by [5]

$$A_p=\rho\frac{\rho(1-\rho)Fr^{-1}+\rho\gamma k^2-(1-\rho)k}{\rho^2(3-\rho)Fr^{-1}+\rho^2\gamma k^2+(1-\rho)(2-\rho)k}\le 0\,,\quad \omega=0\,, \tag{38}$$

and

$$A_p=-\frac{\rho}{1-\rho}\,,\quad \omega^2=k\left[\frac{1+\rho}{1-\rho}Fr^{-1}+\frac{k^2}{1-\rho}\gamma+\frac{k}{\rho}\right]\,, \tag{39}$$

where $k = |\mathbf{k}|$. For $A_p > 0$, the basic solution is always unstable, and thus steady, planar combustion is only stable in the region $A_p < 0$ that lies between these two curves (Fig. 1). The first of these boundaries is a cellular boundary ($\omega = 0$) that corresponds to the classical Landau instability. Indeed, in the limit $A_p = 0$, corresponding to a constant normal burning rate independent of pressure, Landau's classical result is recovered since in the limit that γFr^{-1} approaches the value $(1-\rho)/4\rho^2$ from below, the cellular stability boundary recedes from the region $A_p < 0$. The pulsating stability boundary (39), on the other hand, only occurs for nonzero A_p, and hence was not predicted by the classical theories that assumed a constant normal burning rate. We note that zero and negative values of A_p over certain pressure ranges are characteristic of the HAN-based liquid propellants mentioned above [2].

The formalism necessary to analyze the fully viscous problem is suggested by the fact that, for small ρ, the cellular boundary (38) has different limiting forms dependent on the relative magnitude of k with respect to ρ. Thus, based on characteristic parameter values, we introduce a bookkeeping parameter $\epsilon \ll 1$ and define the scaled parameters g^*, ρ^*, μ^* and A_p^* according to

$$\rho = \rho^*\epsilon\,, \quad \mu = \mu^*\epsilon\,, \quad A_p = A_p^*\epsilon\,, \quad Fr^{-1} = \begin{cases} g \\ g^*\epsilon \end{cases}, \tag{40}$$

where γ and $Pr_l \equiv P$ are regarded as O(1), and the scaling for A_p is motivated by Eq. (38). Here, the lower scaling on Fr^{-1} corresponds to a reduced gravity limit, whereas the upper definition indicates the normal gravity case. Equation (38) then suggests three wavenumber scales; an inner (small) scale k_i, the outer O(1) scale k, and a far outer (large) scale k_f, where the first and last are defined as

$$k_i = \begin{cases} k/\epsilon, & Fr^{-1} \sim \mathrm{O}(1) \\ k/\epsilon^2, & Fr^{-1} \sim \mathrm{O}(\epsilon)\,, \end{cases} \qquad k_f = k\epsilon\,. \tag{41}$$

Thus, in each of these regions, the corresponding leading-order expressions for A_p^* are deduced from Eq. (38) as

$$A_p^{*(i)} \sim \begin{cases} \rho^*(\rho^* g - k_i)/2k_i \\ \rho^*(\rho^* g^* - k_i)/2k_i \end{cases}, \quad A_p^{*(o)} \sim -\frac{1}{2}\rho^*\,, \quad A_p^{*(f)} \sim \frac{1}{2}\rho^*(\rho^*\gamma k_f - 1)\,, \tag{42}$$

and hence a uniformly valid composite expansion $A_p^{*(c)}(k)$ may be constructed as

$$\begin{aligned} A_p^{*(c)} &\sim A_p^{*(i)} + A_p^{*(o)} + A_p^{*(f)} - \lim_{k_i \to \infty} A_p^{*(i)} - \lim_{k_f \to 0} A_p^{*(f)} \\ &\sim -\frac{1}{2}\rho^* + \frac{1}{2}\epsilon\rho^{*2}\gamma k + \begin{cases} \epsilon\rho^{*2} g/2k \\ \epsilon^2\rho^{*2} g^*/2k \end{cases}, \end{aligned} \tag{43}$$

where the definitions of k_i and k_f have been used to express the final result in terms of k. In terms of the original unscaled parameters, Eq. (43) becomes

$$A_p \sim -\frac{\rho}{2} + \frac{\rho^2}{2}\gamma k + \frac{\rho^2}{2k} Fr^{-1}\,, \tag{44}$$

which, in the parameter regime considered, is a leading-order asymptotic representation of the exact relation (38). It is readily deduced from Eqs. (42) – (44), as discussed in further detail elsewhere [6], that surface tension stabilizes large wavenumber disturbances, while gravity stabilizes small wavenumber perturbations. In the reduced-gravity limit, the minimum in the stability boundary is thus shifted to smaller wavenumbers, and thus the hydrodynamic cellular instability becomes a long-wave instability phenomenon (Fig. 2).

Corresponding results may be obtained for the viscous case. However, to deduce the asymptotic forms of both the cellular and the pulsating stability boundaries, it is preferable from the standpoint of tractability to introduce the scalings (40) and appropriate perturbation expansions

for the coefficients b_i directly into Eqs. (27) – (37) for each wavenumber regime, and to obtain the neutral stability boundary in question from the expanded form of those equations. Thus, for the cellular boundary $A_p^*(k)$ [6], we deduce the following expansions and results for each wavenumber regime.

$$(i)\ \ k \sim \mathrm{O}(1): \qquad r \sim r_1\,\epsilon + \cdots, \quad r_1 = \mu^* P k^2\,, \tag{45}$$

$$q \sim q_0 + \cdots, \quad q_0 = \frac{1}{2P}\left(1 + \sqrt{1 + 4P^2k^2}\right), \tag{46}$$

$$b_i \sim b_i^{(-1)}\epsilon^{-1} + b_i^{(0)} + b_i^{(1)}\epsilon + \cdots, \quad i = 2, 8\,, \tag{47}$$

$$b_i \sim b_i^{(0)} + b_i^{(1)}\epsilon + \cdots, \quad i = 1, 3, 4, 5, 6, 7\,, \tag{48}$$

$$A_p = A_p^{*(o)}\epsilon \sim \epsilon(A_0^{*(o)} + A_1^{*(o)}\epsilon + \cdots), \quad A_0^{*(o)} = -\rho^*/2\,. \tag{49}$$

$$(ii)\ \ k = \begin{cases} k_i\epsilon \\ k_i\epsilon^2 \end{cases}: \qquad r \sim \mu^* P k_i^2 \begin{cases} \epsilon^3 + \cdots \\ \epsilon^5 + \cdots \end{cases}, \qquad q \sim \frac{1}{2P} + P k_i^2 \begin{cases} \epsilon^2 + \cdots \\ \epsilon^4 + \cdots \end{cases}, \tag{50}$$

$$b_i \sim \begin{cases} b_i^{(0)} + b_i^{(1)}\epsilon + \cdots \\ b_i^{(1)}\epsilon + b_i^{(2)}\epsilon^2 + \cdots \end{cases}, \quad i = 2, 8\,, \tag{51}$$

$$b_i \sim \begin{cases} b_i^{(1)}\epsilon + b_i^{(2)}\epsilon^2 + \cdots \\ b_i^{(1)}\epsilon^2 + b_i^{(3)}\epsilon^3 + \cdots \end{cases}, \quad i = 1, 3, 4, 5, 6, 7\,, \tag{52}$$

$$A_p = A_p^{*(i)}\epsilon \sim \epsilon(A_0^{*(i)} + A_1^{*(i)}\epsilon + \cdots), \quad A_0^{*(i)} \sim \begin{cases} \rho^*(\rho^* g - k_i)/2k_i \\ \rho^*(\rho^* g^* - k_i)/2k_i\,. \end{cases} \tag{53}$$

$$(iii)\ \ k = k_f/\epsilon: \qquad r \sim r_{(-1)}\,\epsilon^{-1} + \cdots, \quad r_{(-1)} = \frac{1}{2\mu^* P}\left(1 - \sqrt{1 + 4\mu^{*2}P^2k_f^2}\right), \tag{54}$$

$$q \sim q_{(-1)}\,\epsilon^{-1} + \cdots, \quad q_{(-1)} = k_f\,, \tag{55}$$

$$b_i \sim b_i^{(-1)}\epsilon^{-1} + b_i^{(0)} + \cdots, \quad i = 1, 3, 5, 7\,, \tag{56}$$

$$b_i \sim b_i^{(-2)}\epsilon^{-2} + b_i^{(-1)}\epsilon^{-1} + \cdots, \quad i = 2, 4, 6, 8\,, \tag{57}$$

$$A_p = A_p^{*(f)}\epsilon \sim \epsilon(A_0^{*(f)} + A_1^{*(f)}\epsilon + \cdots), \tag{58}$$

$$A_0^{*(f)} \sim -\rho^* + \frac{2\rho^*\mu^* P\left[1 + k_f(\rho^*\gamma + 2\mu^* P + 2\rho^* P)\right]}{4\mu^* P(1 + \rho^* P k_f) - \left[1 - (1 + 4\mu^{*2}P^2k_f^2)^{1/2}\right](\rho^*\gamma + 2\mu^* P)}\,. \tag{59}$$

We observe that the leading-order results (49) and (53) are equivalent to the corresponding inviscid results (42). Thus, to leading order, neither the inner nor the outer wavenumber regimes are influenced by viscous effects, which, to a first approximation, are only significant for large-wavenumber disturbances. This is reflected in the leading-order expression for the cellular stability boundary given by Eqs. (58)–(59), where, among other features, it is readily observed that both the liquid *and* the gas-phase viscosities (through the parameters P and $\mu^* P$, respectively) enter into this expression, reflecting an equal influence of viscous and surface-tension effects on the neutral stability boundary in the large-wavenumber regime. The equal importance of gas-phase viscosity

relative to that of the liquid phase stems from the fact that gas-phase disturbances are, according to Eqs. (56) and (57), larger in magnitude than those in the liquid phase, such that a weak damping of a larger magnitude disturbance is as significant as an O(1) damping of a smaller magnitude disturbance. In the limit $P \to 0$, the inviscid expression (42) is recovered. It is easily shown that $\lim_{k_f \to 0} A_0^{*(f)} = -\rho^*/2$, so that the far outer solution can be matched to the outer solution (49). Indeed, a uniformly valid composite expansion spanning all three wavenumber regimes may be constructed as in the inviscid case, giving the result

$$A_p^{*(c)} \sim -\rho^* + \frac{2\rho^*\mu^* P\left[1+\epsilon k(\rho^*\gamma + 2\mu^* P + 2\rho^* P)\right]}{4\mu^* P(1+\epsilon k\rho^* P) - (\rho^*\gamma + 2\mu^* P)\left[1-(1+4\mu^{*2}P^2\epsilon^2 k^2)^{1/2}\right]} + \frac{\rho^{*2}}{2k}\begin{cases}\epsilon g \\ \epsilon^2 g^*\end{cases}, \quad (60)$$

or, reverting to unscaled parameters,

$$A_p^{(c)} \sim -\rho + \frac{2\rho\mu P\left[1+k(\rho\gamma + 2\mu P + 2\rho P)\right]}{4\mu P(1+k\rho P) - (\rho\gamma + 2\mu P)\left[1-(1+4\mu^2 P^2 k^2)^{1/2}\right]} + \frac{\rho^2}{2k} Fr^{-1}. \quad (61)$$

The cellular stability boundaries, based on Eq. (60) are reproduced in Fig. 3, where only those portions of the curves that lie in the region $A_p^* \leq 0$ are shown. For sufficiently small positive values of A_p, it may be shown that there always exists a positive (real) root $i\omega$ of the dispersion relation, which implies that this region is intrinsically unstable. We note from Eq. (59) that as k_f increases, $A_0^{*(f)}$ increases, intersecting the $A_0^{*(f)} = 0$ axis at the value $k_f = (\rho^*\gamma)^{-1}\left[1-\mu^* P/(\rho^*\gamma + 2\mu^* P)\right]$, which agrees with the inviscid result in the limit $\mu^* P \to 0$. It is readily seen from Fig. 3 that, as in the inviscid case, the essential qualitative difference between the normal and reduced-gravity curves is the location of the critical wavenumber for instability. Specifically, the minimum in the neutral stability boundaries occurs for O(1) values of k under normal gravity, and at $k \sim O(\epsilon^{1/2})$ in the reduced-gravity limit considered here. It is also clear from Fig. 3 that increasing the values of any of the parameters P, $\mu^* P$ or γ serves to shrink the size of the unstable domain through damping of short-wave perturbations. The non-negligible effects of gas-phase viscosity represents an important correction to Levich's original treatment [3] in which these effects were simply assumed to be small. The result (60) – (61) thus synthesizes and significantly extends the classical Landau/Levich results [1,3], not only in allowing for a dynamic dependence of the burning rate on local conditions in the vicinity of the liquid/gas interface, but also in its formal treatment of those processes (surface tension, liquid and gas-phase viscosity) that affect damping of large-wavenumber disturbances.

Asymptotic Analysis of the Pulsating Stability Boundary

As indicated previously, the existence of a nonstationary pressure dependence on the burning rate (i.e., $A_p \neq 0$) leads to the prediction of a pulsating hydrodynamic stability boundary that is absent when such a pressure coupling is neglected, as in the original Landau/Levich theories.

In the inviscid case, this boundary (39) is a straight line that lies below the cellular boundary discussed above, but this is modified under the influence of viscosity, as we shall demonstrate.

For the scalings (40) adopted in the preceding section [in particular, for $P \sim \mathrm{O}(1)$, $\mu \sim \mathrm{O}(\epsilon)$], it turns out that, unlike the cellular stability boundary for which viscous effects only have a leading-order effect in the far outer wavenumber regime, the effects of viscosity have a leading-order effect on the pulsating boundary for O(1) wavenumbers as well. Thus, in the outer wavenumber region, we seek a solution for the dispersion relation in the form

$$i\omega \sim \epsilon^{-1/2}\left(i\omega_0 + i\omega_1\epsilon^{1/4} + i\omega_2\epsilon^{1/2} + \cdots\right), \tag{62}$$

where the leading-order term is suggested by the explicit results for the inviscid case [5, 6], and the expansion in powers of $\epsilon^{1/4}$ is suggested by the expansions for r and q, which, from Eqs. (27) and (28), have the form

$$\begin{gathered} r \sim r_{(1/2)}\epsilon^{1/2} + r_{(3/4)}\epsilon^{3/4} + r_1\epsilon + \cdots, \\ r_{(1/2)} = -i\omega_0\rho^*, \quad r_{(3/4)} = -i\omega_1\rho^*, \quad r_1 = -i\omega_2\rho^* - (\mu^* P k)^2, \end{gathered} \tag{63}$$

$$q \sim q_{(-1/4)}\epsilon^{-1/4} + q_0\epsilon^0 + \cdots, \quad q_{(-1/4)} = \sqrt{i\omega_0/P}, \quad q_0 = \frac{1}{2P}\left(1 + i\omega_1/\sqrt{i\omega_0/P}\right). \tag{64}$$

Corresponding expansions for the coefficients b_i in Eqs. (29) – (37) are determined as

$$b_i = b_i^{(-1)}\epsilon^{-1} + b_i^{(-3/4)}\epsilon^{-3/4} + b_i^{(-1/2)}\epsilon^{-1/2} + \cdots, \quad i = 1, 2, 8, \tag{65}$$

$$b_i = b_i^{(-1/2)}\epsilon^{-1/2} + b_i^{(-1/4)}\epsilon^{-1/4} + \cdots, \quad i = 3, 4, 5, 6, \tag{66}$$

$$b_i = b_i^{(-1/4)}\epsilon^{-1/4} + b_i^{(0)}\epsilon^0 + \cdots, \quad i = 7, \tag{67}$$

where the leading terms in the expansions for b_1, b_2, b_4, b_6 and b_8 are consistent with the inviscid results [5] and the remaining coefficients appear only for nonzero values of P and are conservatively postulated to have the indicated expansions. Substituting these expansions into Eqs. (29) – (37) and equating coefficients of like powers of ϵ, we obtain the leading-order equations/results

$$ik_1\, b_3^{(-1/2)} + ik_2\, b_5^{(-1/2)} + q_{(-1/4)}\, b_7^{(-1/4)} = 0, \tag{68}$$

$$ik_1\, b_4^{(-1/2)} + ik_2\, b_6^{(-1/2)} + r_{(1/2)}\, b_8^{-1} = 0, \tag{69}$$

$$b_2^{(-1)} = -\frac{k}{\rho^*}, \tag{70}$$

$$b_1^{(-1)} = \frac{(i\omega_0)^2}{k}, \tag{71}$$

$$b_8^{(-1)} = -\left(1 + \frac{A_p^*}{\rho^*}\right)\frac{k}{\rho^*}, \tag{72}$$

$$b_1^{(-1)} + b_2^{(-1)} - 2b_8^{(-1)} = 0\,, \tag{73}$$

where Eq. (72) was obtained from the leading-order difference of Eqs. (33) and (34), and the remainder of the leading-order versions of Eqs. (29) – (37) give redundant results. Substituting Eqs. (70) – (72) into Eq. (73), we obtain

$$(i\omega_0)^2 = \frac{k^2}{\rho^*}\left(1 + 2\frac{A_p^*}{\rho^*}\right)\,, \tag{74}$$

and thus $(i\omega_0)^2 \gtrless 0$ for $A_p^* \gtrless -\rho^*/2$, which essentially recovers the leading-order cellular stability boundary (49) for O(1) wavenumbers, but gives no information on the pulsating boundary since $i\omega_0$ is purely imaginary for $A_p^* < -\rho^*/2$. Hence, stability in the latter region is determined by higher-order coefficients in the expansion (62) for $i\omega$.

Continuing with the analysis of the expanded forms of Eqs. (29) – (37), we obtain the second-order equations/results

$$ik_1\, b_3^{(-1/4)} + ik_2\, b_5^{(-1/4)} + q_{(-1/4)}\, b_7^{(0)} + q_0\, b_7^{(-1/4)} = 0\,, \tag{75}$$

$$ik_1\, b_4^{(-1/4)} + ik_2\, b_6^{(-1/4)} + r_{(1/2)}\, b_8^{(-3/4)} + r_{(3/4)}\, b_8^{(-1)} = 0\,, \tag{76}$$

$$b_2^{(-3/4)} = 0\,, \tag{77}$$

$$k\, b_2^{(-1/2)} - q_{(-1/4)} b_7^{(-1/4)} = i\omega_0 k\left(1 - \frac{A_p^*}{\rho^*}\right)\,, \tag{78}$$

$$b_7^{(-1/4)} - \frac{k}{i\omega_0} b_1^{(-3/4)} = i\omega_1\,, \tag{79}$$

$$b_8^{(-3/4)} = 0\,, \tag{80}$$

$$b_1^{(-3/4)} = 2b_8^{(-3/4)} = 0\,, \tag{81}$$

$$b_3^{(-1/2)} = b_5^{(-1/2)} = 0\,, \tag{82}$$

where Eq. (78) was obtained from the sum of Eq. (31) multiplied by ik_1 and Eq. (32) multiplied by ik_2 and the use of Eq. (68), Eq. (80) was obtained from the difference of Eqs. (33) and (34), and Eqs. (82) follow from Eqs. (36) and (37) in conjunction with Eq. (77). From these results and Eq. (68), we thus conclude that

$$b_7^{(-1/4)} = i\omega_1 = 0\,, \quad b_2^{(-1/2)} = i\omega_0\left(1 - \frac{A_p^*}{\rho^*}\right)\,, \tag{83}$$

where the fact that $i\omega_1 = 0$ implies the need to calculate $i\omega_2$ to determine stability in the region $A_p^* < -\rho^*/2$. Proceeding in this fashion, we obtain from the next-order versions of Eqs. (33),

(35), the difference of Eqs. (33) and (34), and the sum of Eq. (36) multiplied by ik_1 and Eq. (37) multiplied by ik_2, the relations

$$b_7^{(0)} - \frac{k}{i\omega_0} b_1^{(-1/2)} + \frac{i\omega_2 + k}{(i\omega_0)^2} k\, b_1^{(-1)} - \rho^* b_8^{(-1)} + \rho^* b_2^{(-1)} = i\omega_2\,, \tag{84}$$

$$b_1^{(-1/2)} + \frac{k}{i\omega_0}(2Pk-1) b_1^{(-1)} + b_2^{(-1/2)} + \frac{2i\omega_0\rho^*}{k} b_2^{(-1)} - 2b_8^{(-1/2)} = -i\omega_0\,, \tag{85}$$

$$-\rho^* b_8^{(-1/2)} + \rho^* b_2^{(-1/2)} + \frac{i\omega_0 \rho^{*2}}{k} b_2^{(-1)} + A_p^* b_2^{(-1/2)} = -i\omega_0\rho^*\,, \tag{86}$$

$$-i\omega_0\rho^* b_8^{(-1)} + k\, b_2^{(-1/2)} + i\omega_0\rho^* b_2^{(-1)} + i\omega_0 b_7^{(0)} - (2Pk-1)\frac{k^2}{i\omega_0} b_1^{(-1)} = 0\,, \tag{87}$$

which, when combined with the expressions for $b_1^{(-1)}$, $b_2^{(-1)}$, $b_8^{(-1)}$, $b_2^{(-1/2)}$ and $i\omega_0$ given above, constitute four equations for the four unknowns $b_1^{(-1/2)}$, $b_7^{(0)}$, $b_8^{(-1/2)}$ and $i\omega_2$. Solving these simultaneous equations, we thus obtain

$$b_7^{(0)} = -2Pk^2, \quad b_1^{(-1/2)} = \left[2Pk + 1 + \frac{A_p^*}{\rho^*} - 2\left(\frac{A_p^*}{\rho^*}\right)^2\right] i\omega_0, \quad b_8^{(-1/2)} = \left[1 - \left(\frac{A_p^*}{\rho^*}\right)^2\right] i\omega_0, \tag{88}$$

$$i\omega_2 = k\left[\left(\frac{A_p^*}{\rho^*}\right)^2 - 2Pk - 1\right]. \tag{89}$$

Equation (89) is the desired result, from which we conclude that $i\omega_2 \lesssim 0$ for $(A_p^*/\rho^*)^2 \lesssim 1 + 2Pk$. Thus, in the region $A_p^* < 0$, $i\omega_2$ vanishes on the boundary

$$A_p^* \sim -\rho^* \sqrt{1 + 2Pk}\,, \tag{90}$$

which is a pulsating boundary (Fig. 4) since, from Eq. (74), $i\omega_0$ is purely imaginary along this curve.

Equation (90) is valid for O(1) wavenumbers, but since it matches to the leading-order inviscid inner pulsating boundary $A_p^* = -\rho^*$ as $k \to 0$, and becomes large in a negative sense as k becomes large, it is clear that Eq. (90) represents the pulsating boundary for arbitrary wavenumbers. That is, for $P \sim \mathrm{O}(1)$, the effects of (liquid) viscosity on the pulsating boundary are, to a first approximation, absent for small wavenumbers, are first felt for O(1) wavenumber perturbations, and are sufficient to move this boundary to larger-magnitude values $A_p^* \sim \mathrm{O}(\epsilon^{-1/2})$ in the far outer wavenumber regime. In contrast, the cellular boundary (60) is unaffected for O(1) and smaller wavenumbers, and is only modified an O(1) amount for $\mathrm{O}(\epsilon^{-1})$ wavenumbers. Thus, the hydrodynamic pulsating boundary is more sensitive to viscous effects than is the corresponding cellular stability boundary. For smaller-magnitude viscosities such that $P = \hat{P}\epsilon \sim \mathrm{O}(\epsilon)$, it may be shown by an analogous calculation (Appendix) that O(1) modifications to the pulsating boundary

then occur in the far outer wavenumber regime according to $A_p^* = -\rho^*\left(1 + 2\hat{P}k_f\right)^{1/2}$, which, in terms of unscaled quantities, is the same as Eq. (90).

Conclusion

The present work has presented a formal asymptotic treatment of hydrodynamic instability for a surface model of liquid-propellant combustion in which burning takes place at the liquid/gas interface. The model itself is based on a synthesized version of the classical models analyzed by Landau [1] and Levich [3], generalized to allow a coupling of the burning rate with the local pressure field [4,5]. The realistic smallness of the gas-to-liquid density ratio proved to be a convenient small parameter upon which to base an asymptotic treatment, resulting in three distinct wavenumber regimes with different physical processes assuming dominance in each. Both cellular and pulsating hydrodynamic stability boundaries are predicted by the present model, the former corresponding to Landau's original notion of hydrodynamic instability, and the latter representing a new prediction arising from the pressure dependence of the burning rate. For the cellular type of instability, it was shown that the gravitational acceleration (assumed to be normal to the undisturbed liquid/gas interface in the direction of the liquid) is responsible for stabilizing long-wave disturbances, whereas surface tension and viscosity are effective in stabilizing short-wave perturbations. In the case of pulsating instability, neither gravity nor surface tension play a leading-order role, and viscous effects are the dominant stabilizing influence. Indeed, for O(1) liquid Prandtl numbers, the stabilizing effects of (liquid) viscosity on pulsating instability are significant for disturbances whose wavenumbers are O(1) and higher. On the other hand, viscous effects are only significant for large wavenumber disturbances in the case of cellular instability, where the influence of gas and liquid viscosity are comparable despite the small ratio of these two parameters. Although the onset of pulsating hydrodynamic instability is predicted to occur only for sufficiently negative values of the pressure-sensitivity coefficient A_p, the persistence of the pulsating stability boundary (in the presence of viscous effects) for small wavenumbers suggests that it should be observable in those types of liquid propellants, such as those based on hydroxylammonium nitrate (HAN) and/or triethanolammonium nitrate (TEAN), that are characterized by negative pressure sensitivities over certain pressure ranges. In connection with this, we note that sloshing behavior has been observed during combustion of certain HAN/TEAN/water mixtures [2], but since nonsteady burning can arise via secondary and higher-order bifurcations in the cellular region [7], as well as from a primary crossing of the pulsating boundary described here, further measurements are generally needed to determine the precise origin of such behavior in any given experiment.

Nomenclature

A	burning rate
A_p	pressure-sensitivity coefficient
b_i	coefficients in perturbation solution ($i = 1, 2, \ldots, 8$)
$\mathbf{e}$	rate-of-strain tensor
Fr	Froude number
g	inverse Froude number (gravitational acceleration)
k	perturbation wavenumber
$\hat{\mathbf{n}}_\mathbf{s}$	unit normal
p	pressure
P, Pr	Prandtl number
q	quantity defined by Eq. (27)
r	quantity defined by Eq. (28)
t	time variable
$\mathbf{u}$	perturbation velocity vector
$\mathbf{v}$	velocity vector
(x, y, z)	moving coordinate system
γ	surface-tension coefficient
ϵ	small bookkeeping parameter
ζ	perturbation pressure
λ	gas-to-liquid thermal diffusivity ratio
μ	gas-to-liquid viscosity ratio
ρ	gas-to-liquid density ratio
ϕ_s	perturbation in location of gas/liquid interface
Φ_s	location of gas/liquid interface
ω	complex perturbation frequency

Subscripts, Superscripts:

i	inner wavenumber regime or integer variable
f	far outer wavenumber regime
l	liquid
g	gas
o	outer wavenumber regime
$*$	scaled quantity

Appendix. The Pulsating Stability Boundary for Small Liquid Prandtl Numbers

For small liquid viscosities such that $P = \hat{P}\epsilon$, and the same scalings (40) as in the $P \sim$ O(1) case analyzed in the main body of the text, the effect of viscosity on the cellular boundary disappears at leading order [$P \to 0$ in Eqs. (60) and (61)], while the effect of viscosity on the pulsating boundary is only significant in the far outer wavenumber regime. In that case, the appropriate expansions analogous to Eqs. (62) – (67) are given by

$$i\omega \sim \epsilon^{-3/2}\left(i\omega_0 + i\omega_1\epsilon^{1/4} + i\omega_0\epsilon^{1/2} + \cdots\right), \tag{91}$$

$$r \sim r_{(-1/2)}\epsilon^{1/2} + \mathrm{O}(\epsilon^{-1/4}), \quad r_{(-1/2)} = -i\omega_0\rho^*, \tag{92}$$

$$q \sim q_{(-5/4)}\epsilon^{-5/4} + \mathrm{O}(\epsilon^{-1}), \quad q_{(-5/4)} = \sqrt{i\omega_0/\hat{P}}, \tag{93}$$

$$b_i = b_i^{(-2)}\epsilon^{-2} + b_i^{(-7/4)}\epsilon^{-7/4} + b_i^{(-3/2)}\epsilon^{-3/2} + \cdots, \quad i = 1, 2, 8, \tag{94}$$

$$b_i = b_i^{(-3/2)}\epsilon^{-3/2} + b_i^{(-5/4)}\epsilon^{-5/4} + \cdots, \quad i = 3, 4, 5, 6, \tag{95}$$

$$b_i = b_i^{(-5/4)}\epsilon^{-5/4} + b_i^{(-1)}\epsilon^{-1} + \cdots, \quad i = 7. \tag{96}$$

Substituting these expansions into Eqs. (29) – (37) and equating terms corresponding to like powers of ϵ then gives, as previously, a sequence of equations for the recursive determination of the coefficients in the above expansions. Similar to the calculation for $P \sim$ O(1) in the outer wavenumber regime, we obtain in this case that

$$(i\omega_0)^2 = \frac{2k_f^2}{\rho^{*2}}\left(A_p^* - \hat{A}_p^*\right), \quad i\omega_1 = 0, \quad i\omega_2 = k_f\left[\left(\frac{A_p^*}{\rho^*}\right)^2 - 2\hat{P}k_f - 1\right], \tag{97}$$

where $\hat{A}_p^* = (\rho^*/2)(\rho^*\gamma k_f - 1)$ is the inviscid cellular boundary in the far outer wavenumber regime given by the last of Eqs. (42). The first of Eqs. (97) thus recovers the cellular stability boundary, but since $i\omega_0$ is purely imaginary for $A_p^* < \hat{A}_p^*$, stability in that region is determined by the real part of the next nontrivial coefficient in the expansion (91). Thus, setting $i\omega_2 = 0$ in the last of Eqs. (97), the pulsating stability boundary in the far outer wavenumber regime is given by

$$A_p^* = -\rho^*\sqrt{1 + 2\hat{P}k_f}, \tag{98}$$

which, in the limit $k_f \to 0$, matches with the leading-order pulsating boundary $A_p^* = -\rho^*$ in the outer wavenumber region, which is unaffected by viscosity to this order of approximation. Thus, Eq. (98), which in terms of k is given by $A_p^* = -\rho^*\left(1 + 2\hat{P}\epsilon k\right)^{1/2}$, is valid for arbitrary wavenumbers. Writing $\hat{P}$ in terms of its unscaled counterpart P, this expression becomes identical to Eq. (90), which thus remains valid in the limit of small P.

Acknowledgement

This work was supported by the United States Department of Energy under the contract DE-AC04-94AL85000 and by the NASA Microgravity Science Research Program under the contract C-32031-E.

References

1. Landau, L. D., "On the Theory of Slow Combustion," *Acta Physicochimica URSS* 19:77–85 (1944), *Zh. Eksp. i Teor. Fiz.* 14:240 (1944).
2. Vosen, S. R., "The Burning Rate of Hydroxylammonium Nitrate Based Liquid Propellants," *Twenty-Second Symposium (International) on Combustion*, The Combustion Institute, Pittsburgh, 1989, pp. 1817–1825.
3. Levich, V. G., "On the Stability of the Flame Front When a Liquid is Burning Slowly," *Dokl. Akad. Nauk SSSR* 109:975–978 (1956).
4. Armstrong, R. C., and Margolis, S. B., "Hydrodynamic and Reactive/Diffusive Instabilities in a Dynamic Model of Liquid Propellant Combustion," *Twenty-Second Symposium (International) on Combustion*, The Combustion Institute, Pittsburgh, 1989, pp. 1807–1815.
5. Armstrong, R. C., and Margolis, S. B., "Hydrodynamic and Reactive/Diffusive Instabilities in a Dynamic Model of Liquid Propellant Combustion—II. Inviscid Fluid Motions," *Combust. Flame* 77:123–138, (1989).
6. Margolis, S. B., "Hydrodynamic Instability in an Extended Landau/Levich Model of Liquid-Propellant Combustion at Normal and Reduced Gravity," *Combust. Flame*, to appear (1998).
7. Bechtold, J. K., and Margolis, S. B., "Nonlinear Hydrodynamic Stability and Spinning Deflagration of Liquid Propellants," *SIAM J. Appl. Math.*, 51:1356–1379 (1991).

Figure Captions

Fig. 1. Hydrodynamic neutral stability boundaries in the limit of zero viscosity.

Fig. 2. Asymptotic representation of the cellular hydrodynamic neutral stability boundary in the limit of zero viscosity. The upper (lower) solid curves correspond to the two cases described by Eqs. (57) for normal and reduced-gravity, respectively (curves drawn for the case $\epsilon = 0.04$, $\rho^* = 1.0$, $g = 2.5$, $g^* = 1.0$).

Fig. 3. Asymptotic representation of the cellular hydrodynamic neutral stability boundary for the viscous case. The upper and lower sets of curves correspond to the normal and reduced-gravity regimes, respectively, in the asymptotic limit considered in this work (curves drawn for the case $\epsilon = .04$, $\rho^* = 1.0$, $g = 6.0$, $g^* = 2.0$). The solid curves correspond to the inviscid limit ($P = 0$) with nonzero surface tension ($\gamma = 2.5$). The dash-dot curves correspond to nonzero surface tension ($\gamma = 2.5$) and liquid viscosity ($P = 1.0$), but zero gas-phase viscosity ($\mu^* P = 0$). The dash-dot-dot curves differ from the dash-dot curves by the addition of gas-phase viscosity ($\mu^* P = 1.0$), and are similar to the dash-dot-dot-dot curves, where the latter correspond to larger viscosities ($P = \mu^* P = 2.0$). The dash-dot-dot-dot-dot curves correspond to a viscous case ($P = \mu^* P = 1.0$), but with zero surface tension ($\gamma = 0$), so that, from Eq. (99), the curves do not intercept the $A_p^* = 0$ axis.

Fig. 4. Asymptotic representation of the pulsating hydrodynamic neutral stability boundary for the viscous case ($P > 0$). The region between the pulsating and cellular boundaries (the latter are shown on an expanded scale in Fig. 3) is the stable region with respect to hydrodynamic instability.

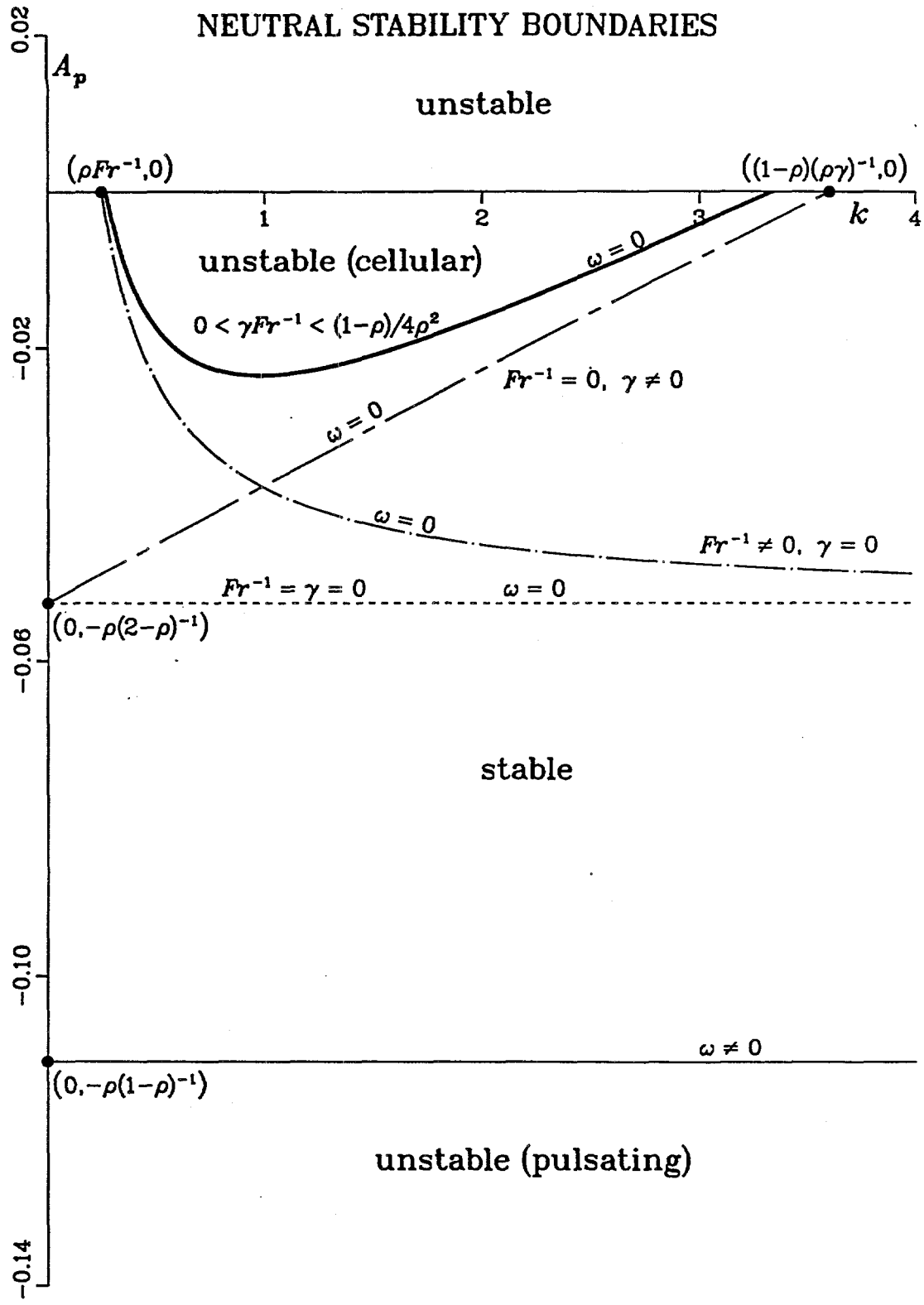
NEUTRAL STABILITY BOUNDARIES
0.02
A_p
unstable
$(\rho Fr^{-1},0)$
$((1-\rho)(\rho\gamma)^{-1},0)$
1
2
3
k
4
unstable (cellular)
$\omega = 0$
$0 < \gamma Fr^{-1} < (1-\rho)/4\rho^2$
$Fr^{-1} = 0,\ \gamma \neq 0$
$\omega = 0$
$\omega = 0$
$Fr^{-1} \neq 0,\ \gamma = 0$
$Fr^{-1} = \gamma = 0$
$\omega = 0$
$(0,-\rho(2-\rho)^{-1})$
−0.02
−0.06
stable
−0.10
$\omega \neq 0$
$(0,-\rho(1-\rho)^{-1})$
unstable (pulsating)
−0.14

Figure 1

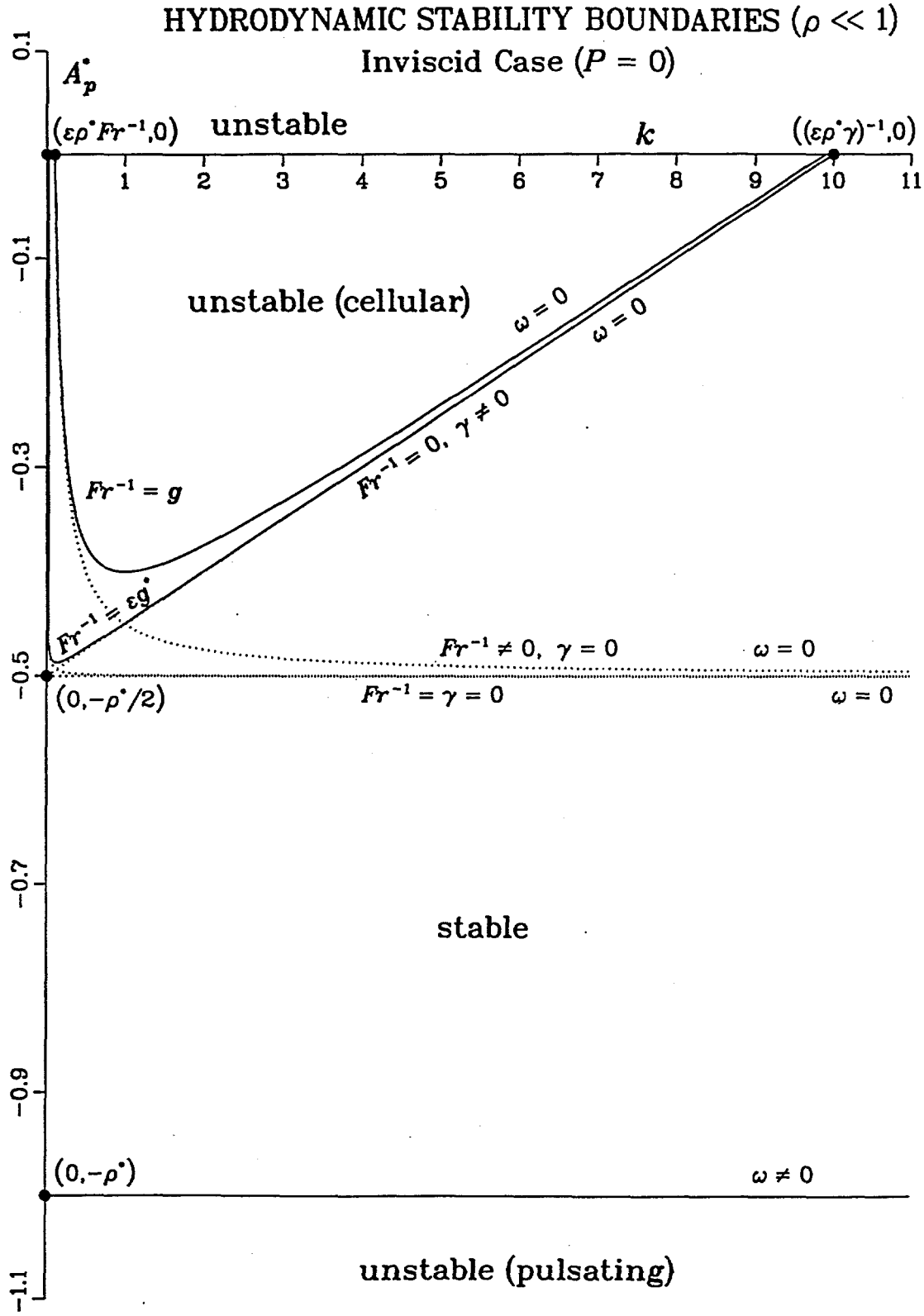
HYDRODYNAMIC STABILITY BOUNDARIES ($\rho \ll 1$)
Inviscid Case ($P = 0$)
A_p^*
$(\varepsilon\rho^* Fr^{-1}, 0)$
unstable
k
$((\varepsilon\rho^*\gamma)^{-1}, 0)$
1
2
3
4
5
6
7
8
9
10
11
0.1
−0.1
−0.3
−0.5
−0.7
−0.9
−1.1
unstable (cellular)
$\omega = 0$
$\omega = 0$
$Fr^{-1} = 0,\ \gamma \neq 0$
$Fr^{-1} = g$
$Fr^{-1} = \varepsilon g^*$
$Fr^{-1} \neq 0,\ \gamma = 0$
$\omega = 0$
$(0, -\rho^*/2)$
$Fr^{-1} = \gamma = 0$
$\omega = 0$
stable
$(0, -\rho^*)$
$\omega \neq 0$
unstable (pulsating)

Figure 2

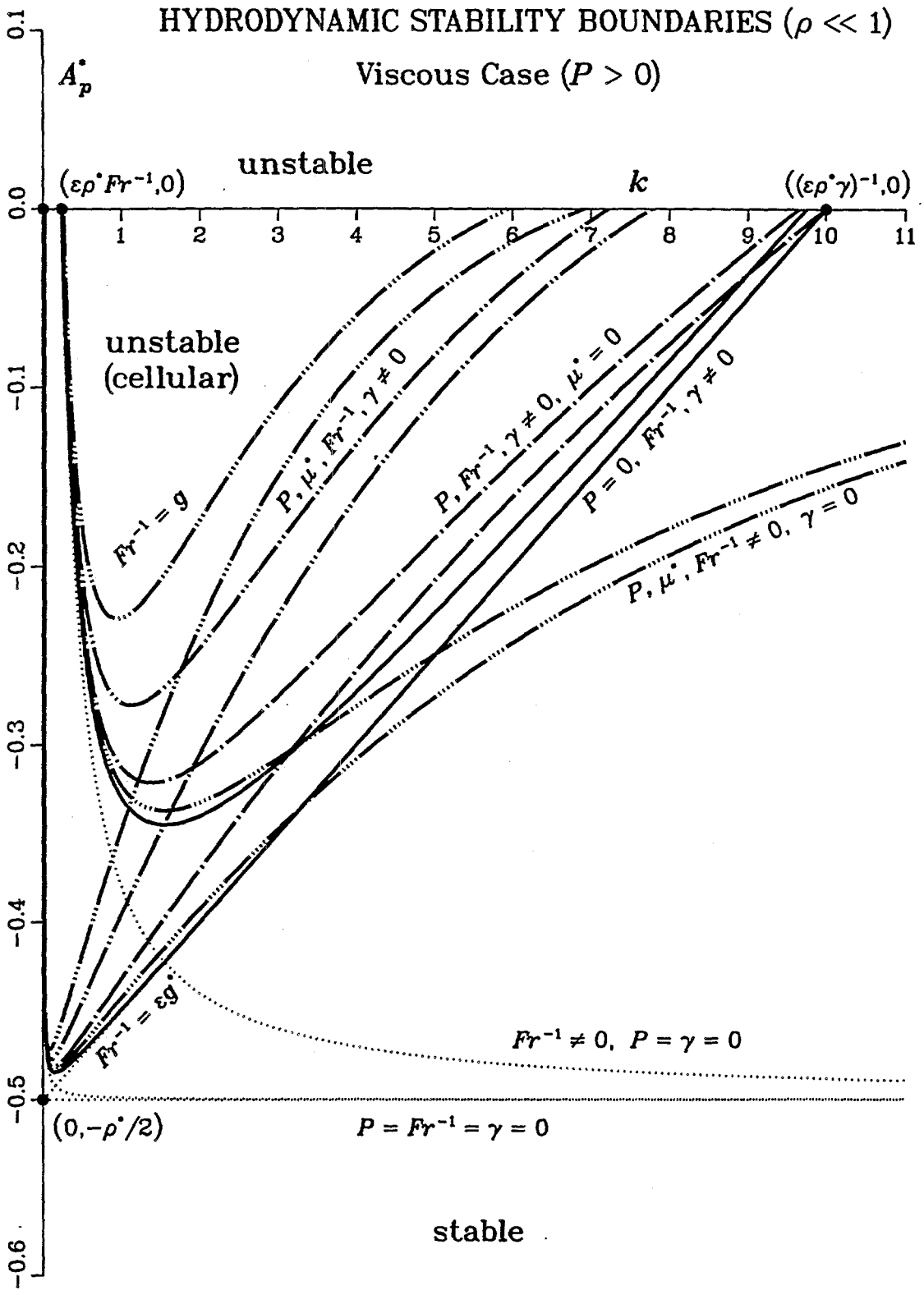
HYDRODYNAMIC STABILITY BOUNDARIES ($\rho \ll 1$)
Viscous Case ($P > 0$)
A_p^*
unstable
$(\varepsilon\rho^* Fr^{-1},0)$
k
$((\varepsilon\rho^*\gamma)^{-1},0)$
unstable
(cellular)
$Fr^{-1} = 9$
$P, \mu^*, Fr^{-1}, \gamma \neq 0$
$P, Fr^{-1}, \gamma \neq 0, \mu^* = 0$
$P = 0, Fr^{-1}, \gamma \neq 0$
$P, \mu^*, Fr^{-1} \neq 0, \gamma = 0$
$Fr^{-1} = \varepsilon g^*$
$Fr^{-1} \neq 0, P = \gamma = 0$
$(0,-\rho^*/2)$
$P = Fr^{-1} = \gamma = 0$
stable

Figure 3

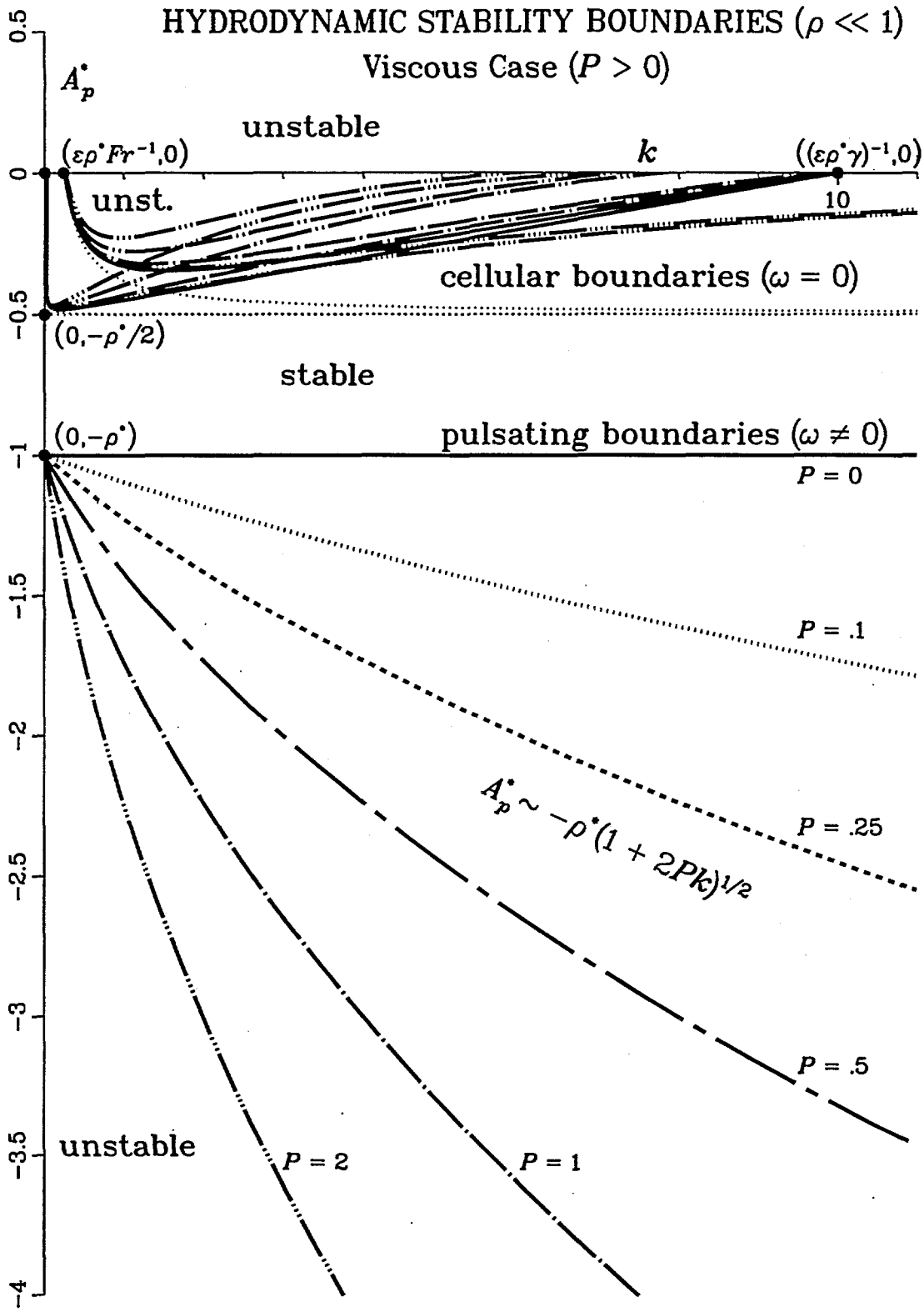
HYDRODYNAMIC STABILITY BOUNDARIES ($\rho \ll 1$)
Viscous Case ($P > 0$)
A_p^*
unstable
$(\varepsilon\rho^* Fr^{-1},0)$
k
$((\varepsilon\rho^*\gamma)^{-1},0)$
unst.
10
cellular boundaries ($\omega = 0$)
$(0,-\rho^*/2)$
stable
$(0,-\rho^*)$
pulsating boundaries ($\omega \neq 0$)
$P = 0$
$P = .1$
$P = .25$
$A_p^* \sim -\rho^*(1 + 2Pk)^{1/2}$
$P = .5$
unstable
$P = 2$
$P = 1$
0.5
0
−0.5
−1
−1.5
−2
−2.5
−3
−3.5
−4

Figure 4

UNLIMITED RELEASE

INITIAL DISTRIBUTION

Dr. John K. Bechtold
Department of Mathematics
New Jersey Institute of Technology
Newark, NJ 07102-1982

Dr. Mitat A. Birkan
Program Manager
Directorate of Aerospace and Engineering Sciences
Department of the Air Force
Bolling Air Force Base, DC 20332-6448

Prof. Michael Booty
Department of Mathematics
New Jersey Institute of Technology
Newark, NJ 07102-1982

Prof. John D. Buckmaster
Department of Aeronautical and Astronautical Engineering
University of Illinois
Urbana, IL 61801

Prof. Sebastien Candel
Ecole Central des Arts et Manufactures
Grande Voie de Vignes
92290 Chatenay-Malabry
FRANCE

Dr. John Card
Department of Mechanical Engineering
Yale University
New Haven, CT 06520

Prof. J. F. Clarke
College of Aeronautics
Cranfield Institute of Technology
Cranfield-Bedford MK43 OAL
ENGLAND

Prof. Paul Clavin
Laboratoire Dynamique et Thermophysique des Fluides
Universite de Provence
Centre Saint Jerome
13397 Marseille Cedex 4
FRANCE

Prof. F. E. C. Culick
Jet Propulsion Center
California Institute of Technology
Pasadena, CA 91125

Prof. Martin Golubitsky
Department of Mathematics
University of Houston
University Park
Houston, TX 77004

Prof. Michael Gorman
Department of Physics
University of Houston
Houston, TX 77004

Dr. Daryl D. Holm
CNLS, MS 457
Los Alamos National Laboratory
Los Alamos, NM 87545

Prof. G. M. Homsy
Department of Chemical Engineering
Stanford University
Stanford, CA 94305

Dr. G. Joulin
Laboratoirie D'Energetique et de Detonique
Universite de Poitiers
Rue Guillaume VII
86034 Poitiers
FRANCE

Dr. Hans Kaper
Applied Mathematics Division
Argonne National Laboratory
9700 S. Cass Ave.
Argonne, IL 60439

Prof. A. K. Kapila
Department of Mathematical Sciences
Rensselaer Polytechnic Institute
Troy, NY 12128

Prof. D. R. Kassoy
Department of Mechanical Engineering
University of Colorado
Boulder, CO 80309

Prof. Joseph B. Keller
Department of Mathematics
Stanford University
Stanford, CA 94305

Prof. Barbara Keyfitz
Department of Mathematics
University of Houston
University Park
Houston, TX 77004

Prof. C. K. Law
Department of Mechanical and Aerospace Engineering
Engineering Quadrangle
Princeton University
Princeton, NJ 08544

Dr. Gary Leaf
Applied Mathematics Division
Argonne National Laboratory
9700 S. Cass Avenue
Argonne, IL 60439

Prof. Amable Liñán
Universidad Politecnica de Madrid
Escuela Tecnica Superior de Ingenieros Aeronauticos
Plaza del Cardenal Cisneros, 3
Madrid - 3
SPAIN

Prof. J. T. C. Liu
Division of Engineering, Box D
Brown University
Providence, RI 02912

Prof. Moshe Matalon
Department of Engineering Sciences and Applied Mathematics
Northwestern University
Evanston, IL 60208

Prof. Bernard J. Matkowsky
Department of Engineering Sciences and Applied Mathematics
Northwestern University
Evanston, IL 60208

Prof. A. C. McIntosh
Department of Fuel and Energy
University of Leeds
Leeds LS2 9JT
United Kingdom

Prof. D. O. Olagunju
Department of Mathematical Sciences
University of Delaware
Newark, DE 19716

Prof. R. E. O'Malley
Department of Applied Mathematics
University of Washington Seattle, WA 98195

Prof. Norbert Peters
Institute fur Allgemeine Mechanik
Technische Hochschule Aachen
Aachen
GERMANY

Prof. Victor Roytburd
Department of Mathematical Sciences
Rensselaer Polytechnic Institute
Troy, NY 12128

Prof. W. A. Sirignano
Office of the Dean
School of Engineering
University of California, Irvine
Irvine, CA 92717

Prof. L. Sirovich
Division of Applied Mathematics, Box F
Brown University
Providence, RI 02912

Prof. G. I. Sivashinsky
Department of Mathematics
Tel-Aviv University
Ramat-Aviv, Tel-Aviv 69978
ISRAEL

Prof. Mitchell D. Smooke
Department of Mechanical Engineering
Yale University
New Haven, CT 06520

Prof. D. Scott Stewart
Department of Theoretical and Applied Mechanics
University of Illinois
Urbana, IL 61801

Prof. C. H. Su
Division of Applied Mathematics, Box F
Brown University
Providence, RI 02912

Prof. Cesar Treviño
Departmento de Termica y Fluidos
Universidad Nacional Autonoma de Mexico
Facultad de Ingenieria
Patios No. 12, Jardines del Sur
MEXICO 23, D.F.

Prof. Vladimir Volpert
Department of Engineering Sciences and Applied Mathematics
Northwestern University
Evanston, IL 60208

Dr. David Weaver
Air Force Rocket Propulsion Laboratory
DYP/Stop 24
Edwards Air Force Base, CA 93523

Prof. Forman A. Williams
Department of Applied Mechanics and Engineering Sciences
University of California, San Diego
La Jolla, CA 92093

Prof. Vigor Yang
Department of Mechanical Engineering
Pennsylvania State University
University Park, PA 16802

Prof. Benn Zinn
Department of Aerospace Engineering
Georgia Institute of Technology
225 North Avenue, NW
Atlanta, GA 30332

C. K. Westbrook, LLNL, L-321

MS 1110 R. C. Allen, 1422
MS 0834 A. C. Ratzel, 9112
MS 0834 M. R. Baer, 9112
MS 0834 M. L. Hobbs, 9112
MS 0834 R. J. Gross, 9112

MS 9001 T. O. Hunter, 8000
MS 9405 R. E. Stoltz, 8008
MS 9004 M. E. John, 8100
MS 9213 S. C. Johnston, 8103
MS 9054 W. J. McLean, 8300
MS 9163 W. Bauer, 8302
MS 9042 C. M. Hartwig, 8345
MS 9056 L. A. Rahn, 8351
MS 9051 W. T. Ashurst, 8351
MS 9051 A. R. Kerstein, 8351
MS 9052 D. R. Hardesty, 8361
MS 9055 R. Behrens, 8361
MS 9052 S. B. Margolis, 8361 (30)
MS 9053 R. W. Carling, 8362
MS 9021 Technical Communications Department, 8815, for OSTI (2)
MS 9021 Technical Communications Department, 8815/Technical Library, MS 0899, 4414
MS 0899 Technical Library, 4414 (4)
MS 9018 Central Technical Files, 8950-2 (3)